

Multistage *ab initio* quantum wavepacket dynamics for electronic structure and dynamics in open systems: Momentum representation, coupled electron-nuclear dynamics, and external fields

Alexander B. Pacheco and Srinivasan S. Iyengar^{a)}

Department of Chemistry and Department of Physics, Indiana University, Bloomington, Indiana 47405, USA

(Received 11 October 2010; accepted 16 December 2010; published online 16 February 2011)

We recently proposed a multistage *ab initio* wavepacket dynamics (MS-AIWD) treatment for the study of delocalized electronic systems as well as electron transport through donor–bridge–acceptor systems such as those found in molecular-wire/electrode networks. In this method, the *full* donor–bridge–acceptor open system is treated through a rigorous partitioning scheme that utilizes judiciously placed offsetting absorbing and emitting boundary conditions. In this manner, the electronic coupling between the bridge molecule and surrounding electrodes is accounted. Here, we extend MS-AIWD to include the dynamics of open-electronic systems in conjunction with (a) simultaneous treatment of nuclear dynamics and (b) external electromagnetic fields. This generalization is benchmarked through an analysis of wavepackets propagated on a potential modeled on an $\text{Al}_{27} - \text{C}_7 - \text{Al}_{27}$ nanowire. The wavepacket results are inspected in the momentum representation and the dependence of momentum of the wavepacket as well as its transmission probabilities on the magnitude of external bias are analyzed. © 2011 American Institute of Physics. [doi:10.1063/1.3534797]

I. INTRODUCTION

Electron transport between donor and acceptor mediated by a bridge has a fundamental role in a wide range of areas. These include biological redox systems,^{1,2} where electron transport through an intervening bridge is central to photosynthesis,^{3–5} enzyme catalyzed reactions, advanced materials including photovoltaics,^{6–16} molecular nanoelectronics,^{17–22} charge transfer in DNA and large biomolecules,^{23–29} and atmospheric and condensed phase systems, where solvated electron chemistry^{30–41} plays an important role. In materials chemistry, active research in molecular electronics has been triggered^{42–49} partly by the possibility of silicon based electronic chip technology tending to its inherent physical limitations and through novel developments in nanofabrication methods.^{50–54} In addition many of the challenges encountered here are also relevant to photovoltaic systems^{6–16} and solar energy conversion and storage.^{55–57} The intensity of current research effort in these areas is due to the expectation that electronic transport properties may be tailored with tools of synthetic and surface chemistry.^{42–45} To this extent, electronic^{58–62} and optical^{63,64} properties of numerous single molecules,^{44,47,65–67} organic self-assembled monolayers,^{68–72} and carbon nanotubes^{73–76} have been the subject of earnest experimental and theoretical pursuit.

In the context of molecular electronics, the donor–bridge–acceptor electron transfer problem is complicated by the fact that external bias and electrode–molecular wire interface coupling converts the molecular junction into an open system dictated by a nonequilibrium flow of electrons proportional to the external bias as well as electrode–molecular wire interface coupling. As a result of such open-system boundary

conditions, the eigenstates of the molecule interact with those of the probe to create a broadened set of states. There exist several computational methods to deal with this problem. Theoretical studies are generally carried out using Landauer's theory and the method of nonequilibrium Green's functions (NEGF).^{42,72,77–101} In addition, recent attempts include the generalization of time-dependent density functional theory to open-system boundary conditions.^{100,102,103}

Toward this end, in Ref. 104, we proposed an approach called the multistage *ab initio* wavepacket dynamics (MS-AIWD) formalism to study electron delocalization and transport in an open system. The method includes partitioning the time-dependent Schrödinger equation for the full donor–bridge–acceptor system into multiple “stages” through *offsetting absorbing and emitting potentials*. The absorbing/emitting potentials are chosen to rigorously cancel, and this allows an exact partitioning of the full system. The offsetting absorbing and emitting potentials describe the coupling between the multiple stages and allow exchange of electron density between the donor, acceptor, and bridge regions. The method in Ref. 104 was inspired by the reactant product decoupling approximation^{105–116} and the use of wavepackets that are narrow in the coordinate representation (and broad in energy and momentum representations)^{117,118} popular in quantum scattering theory. In this paper, we further develop our MS-AIWD method to study electron transport inclusive of electron-nuclear interactions and coupling to external electromagnetic fields. Goals associated with these proposed developments include (a) treatment of nuclear vibrational effects on electron transport in the donor–bridge–acceptor open system. Specifically, current induced forces on the nuclei^{119–122} and the associated vibrational signature of the molecule, inclusive of anharmonic effects, during the nonequilibrium electron transfer process may help understand inelastic electron

^{a)}Electronic mail: iyengar@indiana.edu.

tunneling spectroscopy^{123–127} results and (b) study of temperature dependence of electron transport, when such temperature dependence appears as a result of nuclear motion.

This paper is organized as follows. In Sec. II we provide an overview of the MS-AIWD method. Following this, a detailed formal examination of the “self-energy” that couples the bridge molecule with donor and acceptor regions is provided in Sec. III. Numerical results obtained from the MS-AIWD formalism are then examined in the momentum representation in Sec. IV. This provides new perspectives to analyze the dynamics, and we note subtle effects from the momentum distribution that arise due to changes in the initial wavepacket momentum distribution. These effects are re-examined later in the paper when external fields are introduced. Consequently, generalizations to MS-AIWD that include nuclear dynamics and interaction with external fields are provided in Sec. V. Computational studies are discussed in Sec. VI. These allow the dynamics of open-electronic systems with nuclei in the presence of external AC fields of varying strengths and employ the multistage algorithms presented here. Conclusions are given in Sec. VII.

II. THE MS-AIWD FORMALISM

A. The multistage partitioning scheme

We start with the full time-dependent Schrödinger equation

$$i\hbar \frac{\partial}{\partial t} \Psi(t) = (H + \Delta(t))\Psi(t), \quad (1)$$

where H is the Hamiltonian for the system and contains *all electrons and nuclei in the system* and $\Delta(t)$ is the external bias. We redefine the full Hamiltonian using one-electron absorbing^{128–157} and emitting potentials such that

$$H \equiv H + iV_{I-II} - iV_{I-II} + iV_{II-III} - iV_{II-III} + iV_{II-IV} - iV_{II-IV}. \quad (2)$$

The absorbing potentials V_{I-II} , etc., are localized in space, which allow us to split the system into multiple stages. We consider four stages named I through IV and further partitioning can be carried out if necessary. (See Fig. 1.) Stage I contains the source (semi-infinite donor) region with an absorbing potential (negative imaginary, $\equiv -iV_{I-II}$) at the interface between stages I and II. Similarly, there appears an absorbing potential on the interface of stages II–III and stages II–IV. We denote the wavepacket localized in the stage I region as Ψ_I and similarly for the other stages. Furthermore, as a result of this spatial separation, we require that the full wavefunction be additively described as

$$\Psi(t) \equiv \Psi_I(t) + \Psi_{II}(t) + \Psi_{III}(t) + \Psi_{IV}(t). \quad (3)$$

In our time-dependent approach, the initial wavepacket $\Psi_0(t=0)$ begins deep inside the source electrode. We assume, without loss of generality, that the source is the left electrode. We next exploit the absorbing and emitting potentials, by substituting Eq. (2) into Eq. (1), leading to the equa-

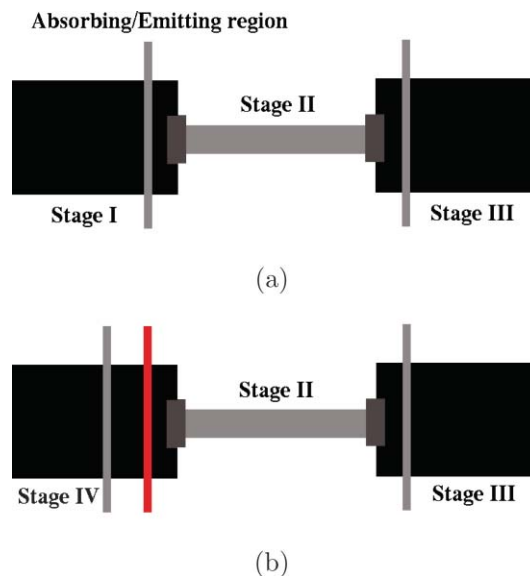


FIG. 1. Part (a) displays a schematic for Stages I–III. The light gray vertical lines represent absorbing potentials introduced between the various stages. For clarity, part (b) displays stages II–IV. As noted in the discussion, the initial wavepacket emanates from stage I, proceeds into stage II, and then either transmits through (stage III) or gets reflected from (stage IV) the molecule that is present in stage II. The red vertical line represents an emitting potential and is placed at the same position as the absorbing potential between stages I and II in part (a). Formally we assume that the absorbing (gray vertical line) and emitting (red) potentials on the left side of part (b) are infinitesimally close. See Eq. (4) and associated discussion on the offsetting absorbing/emitting potentials. To facilitate the discussion in Sec. II, this figure has been reproduced from A. Pacheco and S. S. Iyengar, *J. Chem. Phys.* **133**, 044105 (2010). Copyright 2010, American Institute of Physics.

tions of motions for the partitioned system as

$$(H + \Delta - iV_{I-II})|\Psi_I\rangle = i\hbar \frac{\partial}{\partial t} |\Psi_I\rangle, \quad (4a)$$

$$(H + \Delta - iV_{II-III} - iV_{II-IV})|\Psi_{II}\rangle + iV_{I-II}|\Psi_I\rangle = i\hbar \frac{\partial}{\partial t} |\Psi_{II}\rangle, \quad (4b)$$

$$(H + \Delta)|\Psi_{III}\rangle + iV_{II-III}|\Psi_{II}\rangle = i\hbar \frac{\partial}{\partial t} |\Psi_{III}\rangle, \quad (4c)$$

$$(H + \Delta)|\Psi_{IV}\rangle + iV_{II-IV}|\Psi_{II}\rangle = i\hbar \frac{\partial}{\partial t} |\Psi_{IV}\rangle. \quad (4d)$$

The additive nature of the wavefunction in Eq. (3) allows this separation. Furthermore, the individual stage Hamiltonians in Eq. (4) are non-Hermitian, although the full Hamiltonian in Eq. (1) may be Hermitian and is additively obtained from the Hamiltonians for stages I–IV. If the full Hamiltonian in Eq. (1) includes effects from coupling to an external bath, it would also be non-Hermitian; the individual stage-Hamiltonians however retain their forms listed above. For the cases where the full Hamiltonian is Hermitian, it is also to be noted that any unitarity that may result from the full Hamiltonian in Eq. (1) is also preserved in Eq. (4). That is, the dissipative nature introduced through the partitioning depicted in Eq. (4) is fully contained within the domain of definition of the full Hamiltonian in Eq. (1). This aspect was numerically and formally demonstrated in Ref. 104.

B. Wavepacket propagation for the individual stages

The stage I wavepacket is propagated according to

$$\Psi_I(t) = \exp\left[-\frac{iH_I t}{\hbar}\right] \Psi_I(t=0), \quad (5)$$

where $H_I \equiv (H + \Delta(t) - iV_{I-II})$. The stage I wavepacket density gets accumulated in the region of the absorbing potential as a result of the applied external bias $\Delta(t)$, which is assumed to be slowly varying. The portion of the wavepacket accumulating in the stages I–II absorbing region acts as a source for further propagation into stage II. The solution to the stage II region is obtained using the integrating factor, $\exp[-(i/\hbar)\int_0^t H_{II} dt']$, where $H_{II} \equiv H + \Delta(t) - iV_{II-III} - iV_{II-IV}$, in Eq. (4b),

$$\begin{aligned} \Psi_{II}(t) = & \exp\left[-\frac{i}{\hbar}\int_0^t dt' H_{II}\right] \\ & \times \left\{ \Psi_{II}(0) + \frac{1}{\hbar}\int_0^t dt' \exp\left[-\frac{i}{\hbar}\int_{t'}^0 dt'' H_{II}\right] \right. \\ & \left. \times V_{I-II} \Psi_I(t') \right\}. \quad (6) \end{aligned}$$

If we assume that $\Delta(t)$ is slowly varying with respect to the time step, δt , a propagation scheme for stage II is given by

$$\begin{aligned} |\Psi_{II}(t + \delta t)\rangle = & \exp\left[-\frac{i}{\hbar} H_{II} \delta t\right] \\ & \times \left[|\Psi_{II}(t)\rangle + \frac{\delta t}{2\hbar} V_{I-II} |\Psi_I(t)\rangle \right] \\ & + \frac{\delta t}{2\hbar} V_{I-II} |\Psi_I(t + \delta t)\rangle \quad (7) \end{aligned}$$

or

$$\begin{aligned} |\tilde{\Psi}_{II}(t + \delta t)\rangle = & \exp\left(-\frac{i}{\hbar} H_{II} \delta t\right) |\tilde{\Psi}_{II}(t)\rangle \\ & + \frac{\delta t}{\hbar} V_{I-II} |\Psi_I(t + \delta t)\rangle, \quad (8) \end{aligned}$$

where

$$|\tilde{\Psi}_{II}(t)\rangle = |\Psi_{II}(t)\rangle + \frac{\delta t}{2\hbar} V_{I-II} |\Psi_I(t)\rangle. \quad (9)$$

Note that the first term in Eq. (7),

$$\exp\left[-\frac{i}{\hbar} H_{II} \delta t\right] |\Psi_{II}(t)\rangle, \quad (10)$$

corresponds to unitary evolution in conjunction with dissipative terms, $\{-iV_{II-III} - iV_{II-IV}\}$. The additional source term for stage II may be written using the second and third terms of Eq. (7) as

$$\begin{aligned} & \exp\left[-\frac{i}{\hbar} H_{II} \delta t\right] \left[\frac{\delta t}{2\hbar} V_{I-II} |\Psi_I(t)\rangle \right] + \frac{\delta t}{2\hbar} V_{I-II} |\Psi_I(t + \delta t)\rangle \\ & = \frac{\delta t}{2\hbar} \left\{ \exp\left[-\frac{i}{\hbar} H_{II} \delta t\right] [V_{I-II} |\Psi_I(t)\rangle] \right. \\ & \left. + V_{I-II} \left(\exp\left[-\frac{i}{\hbar} H_I \delta t\right] |\Psi_I(t)\rangle \right) \right\}. \quad (11) \end{aligned}$$

Thus, on the one hand the stage I wavepacket, $|\Psi_I(t)\rangle$, is projected onto the absorbing domain through the action of V_{I-II} and the resultant wavepacket is propagated using the stage II propagation operator, $\exp[-(i/\hbar)H_{II}\delta t]$. (This is seen from the first term on the right side above.) On the other hand, the stage I propagated wavepacket, $|\Psi_I(t + \delta t)\rangle [\equiv \exp[-(i/\hbar)H_I\delta t] |\Psi_I(t)\rangle]$, is also directly filtered through the action of V_{I-II} . These two together constitute the net-source for stage II. Thus, stage I wavepackets from two different time steps simultaneously act as a source for stage II.¹⁰⁴

Equation (6) is the integral form of Eq. (4b). Another differential form of Eq. (6) that is analogous to Eq. (4b) can be written down using a Taylor series expansion for the first term on the right hand side up to first order and combining with the term on the left hand side as¹⁰⁴

$$\begin{aligned} \left(i\hbar\frac{\partial}{\partial t} - H_{II}\right) \Psi_{II}(t) = & \frac{i}{\delta t} \exp\left[-\frac{i}{\hbar} H_{II} \delta t\right] \int_t^{t+\delta t} dt' \\ & \times \exp\left[-\frac{i}{\hbar} H_{II}(t-t')\right] V_{I-II} \Psi_I(t'). \quad (12) \end{aligned}$$

The right side above is, of course, the continuous generalization of the second and third terms in Eq. (7), that is, the terms in Eq. (11), and includes a memory kernel arising from interaction with stage I in this case. *The memory kernel here arises purely as a result of coupling of stage II to the other stages.*

It is further important to note that different kinds of approximate Hamiltonians can be employed to describe stage I, the electrode region, and stage II, the molecule and molecule–electrode interface region. For example, if a uniform electron gas approximation¹⁵⁸ is used to describe the electrode region, this would correspond to the commonly used wide-band approximation.¹⁵⁹ Tight-binding methods can be used as well, and if desired more accurate electronic structure methods can be used. In all the cases the regions of the system are fully coupled as outlined above. Furthermore, as seen in Ref. 104, flow of electronic flux between the different regions is rigorously accounted as a result of the offsetting absorbing and emitting boundary conditions introduced in Eq. (2). Since different quantum mechanical (QM) approximations can be used for the different regions, the approach proposed here belongs to the general class of QM/QM methodologies.^{160–167} But, as noted the partitioning here begins from the time-dependent Schrödinger equation and *exchange of electron density is allowed between the multiple QM regions.*¹⁰⁴

We finally note that the wavepacket densities accumulated in the stages II–III and II–IV absorbing regions are used as source for further propagation into stages III and IV, respectively. Transmission and reflection coefficients are computed from these propagated wavepackets.

1. Backscattering

If the absorbing potentials on either side of stage II are not placed deep inside the electrodes, then there is a possibility of backscattering from stages III and IV into stage II. This could also be the case for systems where there is

a large degree of molecule–electrode coupling. To account for such a backscattering, we modify Eq. (7) by including “source” terms from the back-scattered stage III and stage IV wavepackets as

$$|\tilde{\Psi}_{\text{II}}^B(t + \delta t)\rangle = \exp\left(-\frac{i}{\hbar} H_{\text{II}} \delta t\right) |\tilde{\Psi}_{\text{II}}^B(t)\rangle + \frac{\delta t}{\hbar} |\Psi_{\text{source}}(t + \delta t)\rangle, \quad (13)$$

where

$$|\tilde{\Psi}_{\text{II}}^B(t)\rangle = |\Psi_{\text{II}}^B(t)\rangle + \frac{\delta t}{2\hbar} |\Psi_{\text{source}}(t)\rangle, \quad (14)$$

$$|\Psi_{\text{source}}(t)\rangle = V_{\text{I-II}} |\Psi_{\text{I}}(t)\rangle + V'_{\text{IV-II}} |\Psi_{\text{IV}}(t)\rangle + V'_{\text{III-II}} |\Psi_{\text{III}}(t)\rangle, \quad (15)$$

with $V'_{\text{III-II}}$ and $V'_{\text{IV-II}}$ being the absorbing potentials corresponding to the backscattering from stage III into stage II and stage IV into stage II, respectively, and $|\Psi_{\text{II}}^B(t)\rangle$ is the corrected stage II wavepacket. In other words, the source term for stage II is now modified to include coupling with stages I, III, and IV.

III. THE “SELF-ENERGY,” AS IT ARISES FROM MS-AIWD

It is important to note that the formalism above has a representation of the “self-energy” of the electrode given by the actual interaction term involving the electrode and the electrode–molecule interface. This is because the initial wavepacket for stage II, which was developed by propagation through stage I, contains information about the eigenstates of the electrode in stage I, which is now coupled with the molecular wire in stage II. In case of backscattering, the initial wavepacket for stage II also includes information about the eigenstates of stages III and IV. (See Sec. II B 1.) In this section, we show that the MS-AIWD propagated wavepacket contains information about the “self-energy” interaction with electrodes. This can be seen by choosing the (arbitrary) absorbing and emitting potentials such that

$$V_{\text{II-I}} |\Psi_{\text{II}}\rangle = V_{\text{I-II}} |\Psi_{\text{I}}\rangle \quad (16)$$

inside the domain of definition of $V_{\text{I-II}}$ (the absorbing region between stages I and II) during the time-interval where the source term from stage I is nonzero. Under these conditions there is coupling between stages II and I, and we may rewrite Eq. (4b) as

$$[H + \Delta + iV_{\text{II-I}} - iV_{\text{II-III}} - iV_{\text{II-IV}}] |\Psi_{\text{II}}\rangle = i\hbar \frac{\partial}{\partial t} |\Psi_{\text{II}}\rangle \quad (17)$$

or

$$i\hbar \frac{\partial}{\partial t} |\Psi_{\text{II}}\rangle = [H + \Delta(t) + i\Gamma] |\Psi_{\text{II}}\rangle, \quad (18)$$

where

$$\Gamma = \Gamma_a + \Gamma_d \quad (19)$$

and $\Gamma_d = V_{\text{II-I}} - V_{\text{II-IV}}$, and $\Gamma_a = -V_{\text{II-III}}$. Recognizing that the general solution to the full time-dependent Schrödinger equation comprises a linear combination of waves moving from left to right and those moving right to left,

$$|\Psi_{\text{II}}\rangle = c^L |\Psi_{\text{II}}^L\rangle + c^R |\Psi_{\text{II}}^R\rangle, \quad (20)$$

where $|\Psi^L\rangle$ and $|\Psi^R\rangle$ are the left- and right-moving states, respectively. To obtain $|\Psi_{\text{II}}^R\rangle$, we may reverse the roles of stages I, III, and IV in Eq. (4), which yields

$$i\hbar \frac{\partial}{\partial t} |\Psi_{\text{II}}^L\rangle = [H + \Delta(t) + i\Gamma^L] |\Psi_{\text{II}}^L\rangle, \quad (21a)$$

$$i\hbar \frac{\partial}{\partial t} |\Psi_{\text{II}}^R\rangle = [H + \Delta(t) + i\Gamma^R] |\Psi_{\text{II}}^R\rangle, \quad (21b)$$

and

$$i\hbar \frac{\partial}{\partial t} |\Psi_{\text{II}}\rangle = [H + \Delta(t)] |\Psi_{\text{II}}\rangle + i[\Gamma^L c^L] |\Psi_{\text{II}}^L\rangle + i[\Gamma^R c^R] |\Psi_{\text{II}}^R\rangle, \quad (22)$$

where, following Eq. (19), $\Gamma^L = V_{\text{II-I}}^L - V_{\text{II-IV}}^L - V_{\text{II-III}}^L$ and $\Gamma^R = V_{\text{II-I}}^R - V_{\text{II-IV}}^R - V_{\text{II-III}}^R$, and we have indexed the absorbing/emitting potentials based on the direction of incidence of the initial wavepacket. Since the treatment here is time-dependent, the left- and right-moving states are obtained through choice of the initial wavepacket. That is, to construct left-moving states, the initial wavepacket is to be chosen on the right electrode and emanates toward the target molecule on its left. This is done by reversing the spatial sense of propagation in Eq. (4).

Equations (17), (18), and (22) provide general prescriptions for relating a time-dependent NEGF theory with the MS-AIWD scheme. We stress again that Γ^L and Γ^R are combinations of left and right self-energies, as in Eq. (19). In general, when backscattering is included [see Eq. (13)], these self-energies essentially “damp-out” left- and right-moving waves into and out of the molecular wire region. In this sense, one would expect $\Gamma^L = \Gamma^R = \Gamma^{L/R}$ in most cases and here Eq. (22) would reduce to

$$i\hbar \frac{\partial}{\partial t} |\Psi_{\text{II}}\rangle = [H + \Delta(t)] |\Psi_{\text{II}}\rangle + i\Gamma^{L/R} |\Psi_{\text{II}}\rangle. \quad (23)$$

However, for systems that may display a memory effect or nonlocal interactions, $\Gamma^L \neq \Gamma^R$ and the more general form of Eq. (22) takes into account this effect.

IV. NUMERICAL INSPECTION OF THE MULTISTAGE TIME-DEPENDENT WAVEFUNCTION IN THE MOMENTUM REPRESENTATION

In Ref. 104, we benchmarked the MS-AIWD formalism using a variety of wavepackets differing in widths and initial momenta on an analytical potential modeled on an $\text{Al}_{27} - \text{C}_7 - \text{Al}_{27}$ nanowire. We showed that the MS-AIWD formalism correctly reproduced the dynamics obtained in absence of the partitioning scheme. We also showed that depending on the width of the initial wavepacket, the average momentum of the wavepacket displayed a different behavior.

In this section, we analyze the behavior of the time-dependent wavepacket for this system in the momentum representation. As in Ref. 104, an analytical potential is modeled as Gaussians centered on the nuclear positions of the $\text{Al}_n - \text{C}_7 - \text{Al}_n$ nanowire, with parameters chosen to reproduce the well depths of the electrostatic potential around the nuclei,

$$V(x) = \sum_i \frac{-1}{\sqrt{a\pi}} \exp\left[-\frac{(x-x_i)^2}{a}\right] \quad (24)$$

and

$$a = \begin{cases} 0.2, & \text{C atom} \\ 0.15, & \text{Al atom.} \end{cases} \quad (25)$$

The linear chain of Al_n atoms is considered to be electron reservoirs on either side of the carbon-nanowire. The positions of the nuclei are obtained from a geometry optimization for a molecule with $n = 6$ using B3LYP/6-311++G(d,p) level of theory. Additional Al atoms were then added on either sides of the molecule at distances of 2.8364 Å, which is the shortest distance between two Al atoms in an fcc crystal,¹⁶⁸ to model an $n = 27$ atom system. The initial wavepacket is chosen as a Gaussian centered at x_0 , with width, σ , and initial momentum, P_0 , and has the form

$$\sigma \Psi_{P_0}(x) = \frac{1}{\sqrt{2\pi}\sigma} \exp\left[-\frac{(x-x_0)^2}{2\sigma^2}\right] \times \exp(i P_0 \times x). \quad (26)$$

The absorbing potentials are chosen to have the form,^{129,132,133}

TABLE I. Parameters used for the absorbing potential [Eq. (27)].

V_0	α	$R'_{\text{I-II}}$	$R'_{\text{II-III (IV)}}$	$R'_{\text{left (right) edge}}$
11.6 eV ^a	1.5 Å ⁻¹	-18 Å	+(-)27 Å	-(+)75 Å

^aReference 168.

$$V_{\text{abs}}(R) = \frac{V_0}{1 + \exp(\alpha * (R - R'))}, \quad (27)$$

where R' defines the boundary plane between the stages. Ideally, V_0 should be equal to the Fermi energy level of the respective electrode so that at a distance R' , the potential reduces to half the Fermi energy level of the electrode. A slow decaying potential is obtained using a smaller value for α , and due to the long tail a considerable portion of the electrode should be included in addition to the wire and contacts. The values used for the parameters in Eq. (27) can be found in Table I. In addition, Fig. 2 provides an illustration of the problem.

In Fig. 3, we provide the initial ($t = 0$ fs), final ($t = 5$ fs), and average wavepacket density distributions in the momentum representation. The average wavepacket density, $\rho_{\text{av}}(P_x) \equiv \chi_{\text{av}}^*(P_x)\chi_{\text{av}}(P_x)$, is calculated from the average

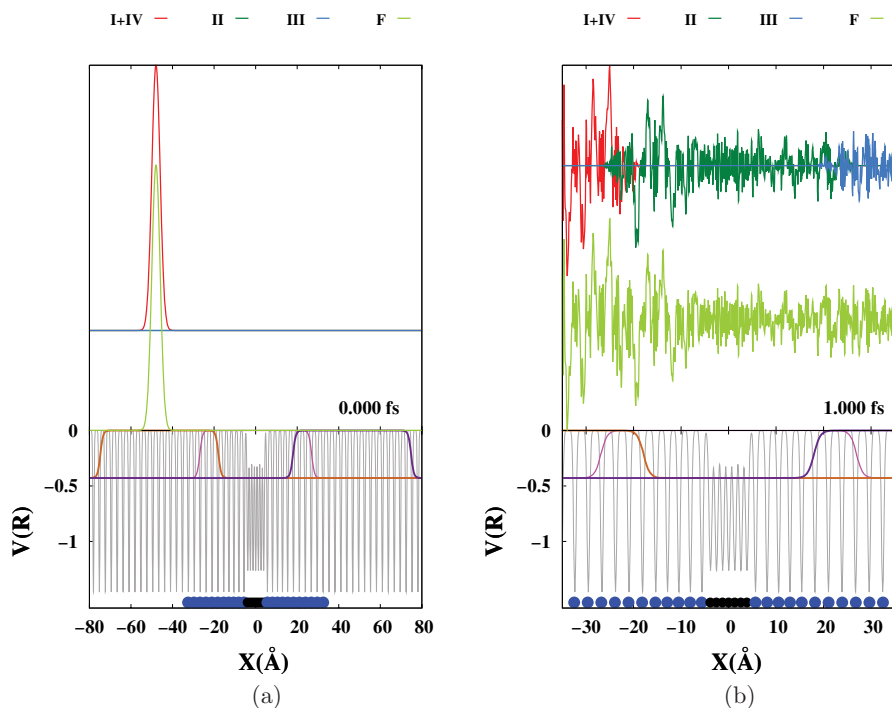


FIG. 2. The model system comprises aluminum atoms (a few of which are depicted using blue solid circles) as electrodes and carbon atoms (black solid circles) as the bridge molecule. The potential [Eq. (26)] is shown in the bottom panel in gray and the absolute value of the absorbing and emitting potentials [Eq. (27)] are shown as decay functions superimposed on the potential. The initial wavepacket is shown on the top panel of (a) and the multistage wavepackets, labeled as I + IV, II, and III, to represent stages I-IV, are shown at 1 fs time into the dynamics in (b). The top panel of both figures also shows the full wavepacket that is obtained when the multistage partitioning scheme is not used. As seen in Ref. 104, these agree well with the multistage wavepackets.

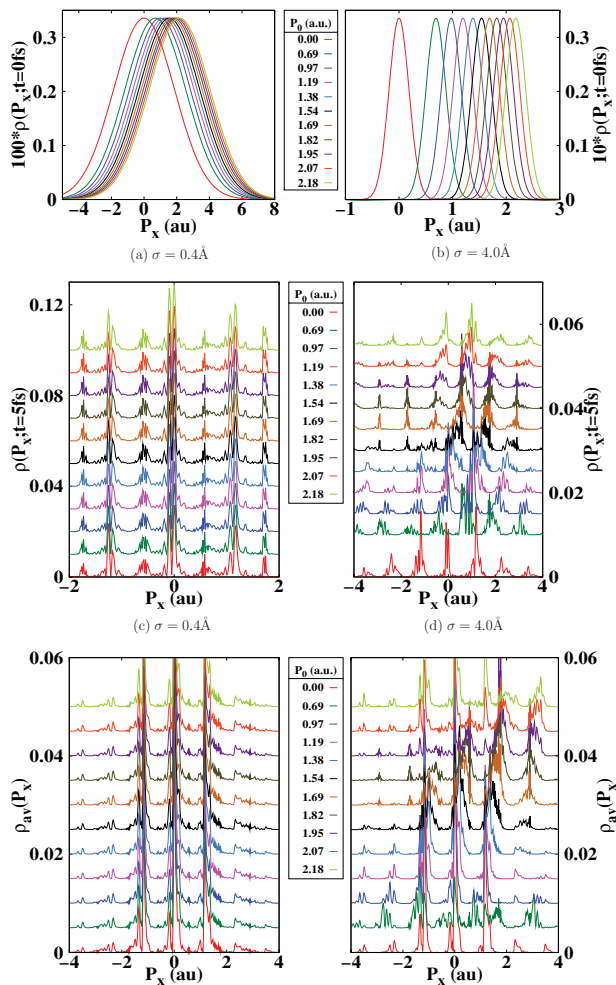


FIG. 3. Wavepacket density in the momentum representation at time [(a) and (b)] 0 fs, [(c) and (d)] 5 fs, and [(e) and (f)] dynamical average [Eq. (28)]. Parts (a), (c), and (e) describe the dynamics of an initial wavepacket that is narrow in the coordinate representation, with $\sigma = 0.4 \text{ \AA}$ in Eq. (26), whereas parts (b), (d), and (e) represent a wider initial wavepacket with $\sigma = 4.0 \text{ \AA}$ in Eq. (26). The $\sigma = 0.4 \text{ \AA}$ wavepackets have a wider momentum distribution (a) and hence sample a similar set of momentum eigenstates and display similar dynamics [(c) and (e)]. The $\sigma = 4.0 \text{ \AA}$ initial wavepackets on the other hand have a narrower momentum distribution (b) and sample completely different momentum eigenstates during the dynamics which is further highlighted in Fig. 4.

wavepacket in the momentum representation,

$$\chi_{\text{av}}(P_x) = \frac{1}{T} \int_0^T dt \int_{-\infty}^{\infty} dx e^{iP_x x/\hbar} \Psi(x; t), \quad (28)$$

where $\Psi(x; t)$ is the wavepacket in the coordinates representation. The time evolution in the momentum representation is presented in Fig. 4.

All wavepackets with broad initial momentum distribution [Figs. 3(a), 3(c), 3(e), and 4(a)–4(d)] sample approximately the same set of momentum eigenstates. This is seen from the rather similar distributions in Figs. 3(c) and 3(e) as a function of initial momentum and the strong emergence of the 0 a.u. and $\approx \pm 1.8$ a.u. momentum peaks in Figs. 3(e) and 4(a)–4(d). Hence the behavior of these initial wavepackets is not very different from each other.

This is, however, not the case for the wavepackets with narrow initial momentum distribution [Figs. 3(b), 3(d), 3(f),

and 4(e)–4(h)]. First, there is a marked difference between the behavior of the narrow and wide initial wavepackets. The wavepackets with narrow initial momentum distribution are “almost pure momentum eigenstates” at the initial time step (since they are narrow in the momentum representation) and sample different sets of momentum eigenstates. [Compare Figs. 3(a) and 3(b).] As a result, these disperse substantially upon impinging the potential which is seen from the pronounced structure in Figs. 4(e)–4(h). Thus the difference in sampling in the initial momentum distribution yields very different time-dependent behavior. Compare the fact that the different wavepackets in Figs. 3(d) and 3(f) have very different behavior with respect to each other. For example, the peaks in Fig. 4(h) appear to emanate from a 2.0 a.u. momentum [which is consistent with the initial momentum distribution for the 2.18 a.u. curve in Fig. 3(b)] and disperse substantially with time, leading to a large spreading of the wavepacket in the momentum representation. This is certainly not the case for the wavepackets with broad initial momentum distributions. The relatively symmetric initial structure of contributions from the momentum representation to the wide wavepacket density results in an equal number of positive and negative momentum states sampled during the dynamics. The absence of such a symmetry for the narrow wavepackets results in a complex momentum distribution.

In fact, due to this complex behavior one does not expect a monotonic (or Ohmic-like) behavior of the average momentum as a function of initial momentum for the narrow initial wavepacket case. This aspect was seen in Ref. 104. (See Fig. 10(a) in Ref. 104, which is reproduced here in Fig. 5 for completeness.) The non-Ohmic portion of this result, that is the portion of green curve in Fig. 5 that depicts a negative slope for the average momentum as a function of initial momentum, appears to be similar to that noted in negative differential resistance^{71,169} studies. This is the case when one notes that an external electric field directed along the axis of the wire would have a first order effect of modifying the momentum of the initial wavepacket. Indeed, we find similar results in Sect. VI C, where external fields are included in the MS-AIWD. These physical results arise due to a nonmonotonic distribution of transmission amplitude (and hence average momentum) as a function of external bias (and hence initial momentum). This aspect is already seen in the simple system depicted here purely due to the sharpness of the initial wavepacket in the momentum representation.

In Sec. V, we generalize MS-AIWD to include effect of nuclear motion and effect of external fields.

V. COUPLED ELECTRON-NUCLEAR DYNAMICS FOR OPEN-ELECTRONIC SYSTEMS IN THE PRESENCE OF EXTERNAL FIELDS

We first discuss generalizations to include nuclear dynamics. Following this, we incorporate external fields.

The full Hamiltonian, H , for coupled electron-nuclear dynamics of the donor–bridged–acceptor system may be

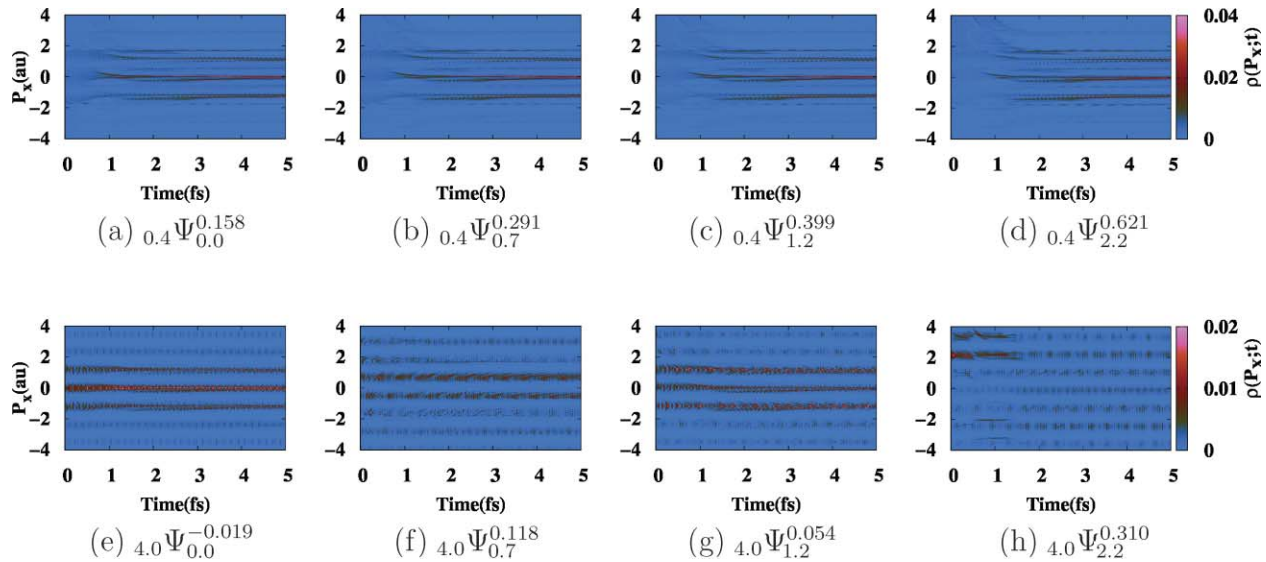


FIG. 4. Contour maps of wavepacket density evolution in time in the momentum representation. The subfigures depict the initial wavepacket configuration. In addition to the notation in Eq. (26), the subfigure indices include the average momentum [in atomic units (a.u.)] on the superscript. The dominant momentum eigenstates that contribute to dynamics differ strongly between the narrow and wide wavepackets.

expanded about a local minimum for the nuclear framework as

$$H = \sum_{\zeta=1}^N \frac{-\hbar^2}{2M_{\zeta}} \nabla_{\zeta}^2 + \sum_{i=1}^n \frac{-\hbar^2}{2m_e} \nabla_i^2 + \sum_{\zeta, \zeta'} \Delta R_{\zeta}^{\top} k_{\zeta \zeta'} \Delta R'_{\zeta} + \sum_{i, \zeta} V(r_i, R_{\zeta}), \quad (29)$$

where the first two terms are the kinetic energy operators for the nuclei and electrons, respectively, and the third term is the interaction between the nuclei expressed as a second order Taylor series expanded about a local minimum, i.e., within the harmonic approximation. Correspondingly, $k_{\zeta \zeta'}$ is the Hessian matrix and the last term is the electron-nuclear potential. We make an assumption that the rotational and translational degrees of freedom are small and can be neglected. If this is not the case, suitable additional degrees of freedom can be included. In addition, in this particular study, we assume the effect of anharmonicity in nuclear motion to also be negli-

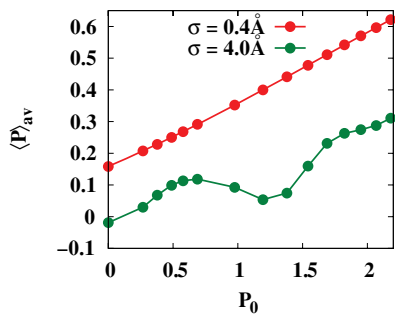


FIG. 5. Time average of the expectation values of the wavepacket momentum, $\langle P \rangle_{av} = 1/T \int_0^T dt \langle \chi(t) | \hat{p} | \chi(t) \rangle$ as a function of initial wavepacket momentum, P_0 , and width, σ , in the coordinate representation [Eq. (26)] in atomic units. This figure has been reproduced from A. Pacheco and S. S. Iyengar, J. Chem. Phys. **133**, 044105 (2010). Copyright 2010, American Institute of Physics.

ble. In these cases, we can then express the Hamiltonian in terms of the $3N - 6$ nuclear degrees of freedom ($3N - 5$ for linear systems) within the harmonic approximation. We then write the Hamiltonian for an electron wavepacket interacting with the nuclei in terms of the generalized normal mode coordinates as

$$H = \frac{1}{2} \sum_{i=1}^{3N-x} (\dot{Q}_i^2 + k_i Q_i^2) - \frac{\hbar^2}{2m_e} \nabla^2 + \sum_{\zeta=1}^{3N} V(r, R_{\zeta}), \quad (30)$$

where x is either 5 or 6 depending on the linear or non-linear case. The mass weighted Cartesian coordinates, $\{\mathcal{R}_{\zeta} \equiv \sqrt{M_{\zeta}} R_{\zeta}\}$, are related to the generalized normal mode coordinates through a transformation matrix as

$$\Delta \mathcal{R}_{\zeta} = (\mathcal{R}_{\zeta} - \mathcal{R}_{\zeta}^{(0)}) = \sum_i A_{\zeta i} Q_i \quad (31)$$

or

$$\Delta R_{\zeta} = (R_{\zeta} - R_{\zeta}^{(0)}) = \sum_i \frac{A_{\zeta i}}{\sqrt{M_{\zeta}}} Q_i = \sum_i A_{\zeta i} Q_i, \quad (32)$$

and $R_{\zeta}^{(0)} = \mathcal{R}_{\zeta}^{(0)} / \sqrt{M_{\zeta}}$ is the equilibrium position of the ζ coordinate.

In this paper we utilize the Ehrenfest dynamics^{170–179} approach to treat the dynamics of the open system electrons and nuclei. The resultant equations of motion for open system electrons and nuclei are

$$i\hbar \frac{\partial}{\partial t} \psi_e(r; t) = H_e \psi_e(r; t), \quad (33)$$

with $H_e = \langle \psi_n(R; t) | H | \psi_n(R; t) \rangle$ and

$$\begin{aligned} \ddot{Q}_i &= \dot{P}_i = -\frac{\partial V_n}{\partial Q_i} - \sum_{\zeta} \frac{\partial R_{\zeta}}{\partial Q_i} \frac{\partial V_e(R_{\zeta})}{\partial R_{\zeta}} \\ &= -k_i Q_i - 2 \sum_{\zeta} \frac{A_{\zeta i}(r - R_{\zeta})}{\sqrt{M_{\zeta}}} \frac{\partial V_e(R_{\zeta})}{\partial R_{\zeta}}, \end{aligned} \quad (34)$$

where

$$V_n = \frac{1}{2} \sum_{i=1}^{3N-5} k_i Q_i^2, \quad (35)$$

$$V_e(R_\zeta) = \langle \psi_e(r; t) | V(r, R_\zeta) | \psi_e(r; t) \rangle, \quad (36)$$

and we use Eq. (24) for the electronic potential in the numerical section of this paper. The electronic potential now becomes time-dependent as a result of nuclear motion, which is noted below.

The position and momenta of the nuclei are propagated using the velocity verlet^{180,181} algorithm

$$\dot{Q}_i(t + dt) = \dot{Q}_i(t) + \frac{dt}{2} [\ddot{Q}_i(t + dt) + \ddot{Q}_i(t)], \quad (37)$$

$$Q_i(t + dt) = Q_i(t) + \dot{Q}_i(t) dt + \frac{dt^2}{2} \ddot{Q}_i(t). \quad (38)$$

The propagated nuclear positions are then used to construct a new electron-nuclear potential using the transformation in Eq. (32). The electron wavepacket is subsequently propagated, using the MS-AIWD scheme outlined earlier in this paper, and the resulting wavepacket averaged potential is used to compute forces on the nuclei for the next propagation step. Thus, the electron wavepacket is propagated on a time-dependent potential coupled to nuclear motion constructed within the harmonic approximation.

To account for the effect of external fields on the electron-nuclear dynamics in open-systems, we invoke the dipole approximation.^{182,183} Here the electronic Hamiltonian is modified according to

$$\begin{aligned} H_e &= \sum_{i=1}^n \frac{1}{2m_e} \left(i\hbar \nabla_i - \frac{e}{c} \mathbf{A} \right)^2 + V_e + e\phi \\ &= \underbrace{\sum_{i=1}^n \frac{-\hbar^2}{2m_e} \nabla_i^2 + V_e}_{H_e^0} - \underbrace{\sum_{i=1}^n \left[\frac{ie\hbar}{2m_e c} \nabla_i \cdot \mathbf{A} + \frac{ie\hbar}{m_e c} \mathbf{A} \cdot \nabla_i \right]}_{H'} + \frac{e^2}{2m_e c^2} |\mathbf{A}|^2 + e\phi, \end{aligned} \quad (39)$$

where \mathbf{A} and ϕ are the vector and scalar potentials, respectively, and V_e is electron-nuclear interaction potential defined in Eq. (36). We have assumed in this paper that the field affects nuclear motion to a lesser extent as compared to the electronic wavepacket. This approximation can be lifted in future through application of a wavepacket description of nuclei.¹⁸⁴⁻¹⁸⁸ Using the Coulomb gauge followed by a transformation where the 4-vector gradient of $[-\vec{r} \cdot \mathbf{A}]$ is zero, i.e., $\square[-\vec{r} \cdot \mathbf{A}] \equiv 0$, we obtain

$$\begin{aligned} H' &= e \frac{2\omega |A_0|}{c} \vec{\epsilon} \cdot \vec{r} \cos(\omega t - \phi) \\ &= e E_0 \vec{\epsilon} \cdot \vec{r} \cos(\omega t - \phi), \end{aligned} \quad (40)$$

which also defines E_0 . Here, we utilize this perturbation term in the electronic Hamiltonian within the MS-AIWD approximation.

VI. NUMERICAL TESTS FOR COUPLED ELECTRON-NUCLEAR MS-AIWD DYNAMICS UNDER THE INFLUENCE OF ELECTROMAGNETIC FIELDS

Here, we benchmark the MS-AIWD formalism inclusive of coupled electron-nuclear dynamics and applied electromagnetic AC fields of varying strengths. However, before we proceed, in Sec. VI A we briefly describe an efficient implementation of our quantum propagation scheme with more details in the Appendix. This discussion is particularly critical to the computational implementation as a result of the highly delocalized electron distribution dynamics. Following this, benchmarks inclusive of coupled nuclear dynamics

are provided in Sec. VI B and dynamics of the electronic open system in the presence of external fields is provided in Sec. VI C.

A. Numerical propagation of the electronic wavepacket using “distributed approximating functionals” (DAFs)

The time evolution of the wavepacket $\Psi(R_{QM}, t)$ is approximated using the symmetric split operator approach

$$\begin{aligned} \exp \left\{ -\frac{iHt}{\hbar} \right\} &= \exp \left\{ -\frac{i\tilde{V}t}{2\hbar} \right\} \exp \left\{ -\frac{iKt}{\hbar} \right\} \\ &\times \exp \left\{ -\frac{i\tilde{V}t}{2\hbar} \right\} + \mathcal{O}(t^3), \end{aligned} \quad (41)$$

where the potential, \tilde{V} , includes the electron-nuclear coupling term, V_e in Eq. (39), the perturbation due to external field, H' in Eq. (39), and the offsetting absorbing/emitting potentials introduced in MS-AIWD. The quantity K is the kinetic energy operator. The free propagation of the wavepacket is represented here using distributed approximating functional (DAF) (Refs. 189 and 190) and is given by^{184,185}

$$\begin{aligned} \Psi(R_{QM}^i; t + \Delta t) &= \exp \left\{ -\frac{iK\Delta t}{\hbar} \right\} \Psi(R_{QM}^j; t) \\ &\equiv \tilde{K}_{\sigma'(0), M_{\text{DAF}}} (R_{QM}^i - R_{QM}^j; \Delta t) \Psi(R_{QM}^j; t) \\ &= \frac{1}{\sqrt{2\pi\sigma'(0)}} \sum_j \exp \left\{ -\frac{(i-j)^2}{2\{\sigma'(\Delta\tau)\}^2} \right\} \end{aligned}$$

$$\begin{aligned} & \times \sum_{n=0}^{M_{\text{DAF}}/2} \left(\frac{\sigma'(0)}{\sigma'(\Delta\tau)} \right)^{2n+1} \left(\frac{-1}{4} \right)^n \\ & \times \frac{1}{n!} H_{2n} \left(\frac{i-j}{\sqrt{2}\sigma'(\Delta\tau)} \right) \Psi(R_{\text{QM}}^j; t), \end{aligned} \quad (42)$$

where $(R_{\text{QM}}^i - R_{\text{QM}}^j) = (i - j)\Delta x$, $\Delta\tau = \Delta t_{\text{QM}}/M_{\text{QM}}(\Delta x)^2$, Δx is the grid discretization in one dimension, H_{2n} are even order Hermite polynomials, and the time dependent (complex) width of the Hermite functions is given by

$$\{\sigma'(\Delta\tau)\}^2 = \{\sigma'(0)\}^2 + i\Delta\tau\hbar. \quad (43)$$

Here, $\sigma(0) = \Delta x\sigma'(0)$ is the width of the initial wavepacket. The parameters M_{DAF} , $\sigma(0)$, Δx , Δt , and M_{QM} determine the accuracy and width of the DAF. The parameters M_{DAF} and $\sigma'(0)$ are coupled, and it has been shown^{191–194} that for a given value of M_{DAF} , there exists a $\sigma'(0)$ that provides optimal accuracy for the propagation. Multidimensional forms of the above propagator are obtained through direct product.

It is worth noting a few characteristics of Eq. (42). For any fixed level of approximation, determined by the choice of parameters M_{DAF} and $\sigma'(0)$, the kernel in Eq. (42) only depends on the quantity $(R_{\text{QM}}^i - R_{\text{QM}}^j)$ that is the distance between points in the coordinate representation and goes to zero as this quantity becomes numerically large on account of the Gaussian dependence. This yields a banded matrix approximation to Eq. (42), for any finite M_{DAF} and $\sigma'(0)$. Furthermore, on account of its dependence on $(R_{\text{QM}}^i - R_{\text{QM}}^j)$, a matrix representation of Eq. (42) has the property that all diagonal elements of this matrix are equal; similarly, all n th super and subdiagonal elements are the same. Such a matrix is called a Toeplitz matrix. On account of such attractive mathematical properties, Eq. (42) provides great simplicity in computation of the quantum propagation. An efficient implementation of the associated propagation scheme is discussed in the Appendix. Furthermore, the accuracy of the DAF approximation has been actively benchmarked in Refs. 191 and 192. It has been shown to compare favorably with other propagation schemes. Specifically, the accuracy of the propagation scheme has been demonstrated in Ref. 192 for the reactant product decoupling approximation of quantum scattering theory which is a basis for the MS-AIWD formalism.

B. Benchmarks on coupled electron-nuclear dynamics for open systems

The model system considered is described in Sec. IV. Additional parameters used in our study can be found in Table II. The $3N - 5$ normal mode displacement vectors obtained from the frequency calculation on the cluster provide the transformation matrix between the normal mode coordinates and the Cartesian coordinates, as given by Eq. (32). Equations (33) and (34) are solved simultaneously where the nuclei are propagated using Eqs. (37) and (38) in an average potential due to the electron wavepacket. The electron wavepacket is propagated within the MS-AIWD formalism with simultaneous evolution of nuclear positions, as given by

TABLE II. List of parameters used for propagation, potential, and wavepacket description used for the benchmark calculations.

(a) Dynamics parameters			(b) Initial wavepackets		
M_{DAF}	Δx	$\sigma'(0)$	Gridpoint	$0.4\Psi_0$	$0.4\Psi_0$
60	0.04 Å	2.574	4001	x_0	-48 Å
				$\sigma/\text{Å}$	0.4 4.0

Eq. (38). This results in a time-dependent potential acting on the electron wavepacket.

In Fig. 6 we provide the evolution of the nuclear potential [Eq. (35)], kinetic, and total energies with respect to their dynamical average. The potential and kinetic energies vary in a similar fashion, and this results in variance in total classical energy of the order of a few ten microhartree. The total energy for the complete electron-nuclear system is well conserved for the duration of the dynamics, where the wavepacket is localized within the grid and does not enter the dissipative, absorbing potentials at either ends of the grid. (See Table I for the positions of absorbing regions.) The nuclear dynamics is conservative to a lesser extent; we use force correlation functions below to gauge the coupling and exchange of energy between the nuclear degrees of freedom and the open-electronic system. In addition, the potential and kinetic energies oscillate with a time period of 0.15 fs superimposed on a larger time period of 3 fs. The amount of energy transferred into the nuclear subsystems is quantified by calculating by the force correlation function for the nuclear motion since this quantity is directly proportional to the electron-phonon coupling matrix elements,¹⁹⁵

$$\mathcal{F}(\omega) \propto \int_{-\infty}^{+\infty} dt e^{-i\omega t} \langle \mathbf{F}(t)\mathbf{F}(0) \rangle, \quad (44)$$

where $\vec{F}_i(t) = -dV(\vec{R}; t)/d\vec{R}_i(t)$ is the force on the i th nuclei and V is the total potential on the classical nuclei given as the sum of Eqs. (35) and (36). In Fig. 7, we provide the force correlation function, $\mathcal{F}(\omega)$, in two energy regimes. The oscillations in the classical potential energy with time periods at 0.15 and 3 fs described earlier appear as peaks in the force

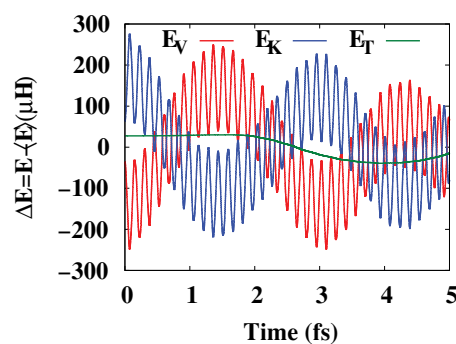


FIG. 6. Evolution of the potential (red), kinetic (blue), and total (green) energies for the nuclei with respect to the dynamical average for the narrow wavepacket ($\sigma = 0.4$ Å) in the absence of external AC fields. The behavior for the broad wavepacket ($\sigma = 4.0$ Å) is qualitatively similar.

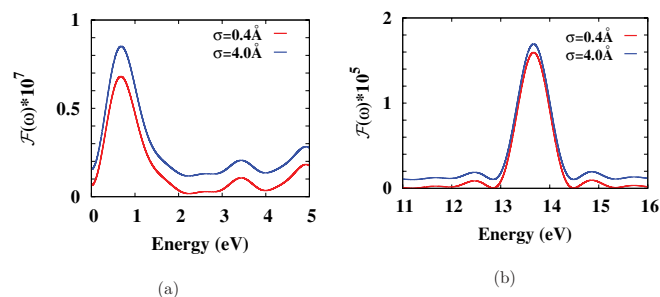


FIG. 7. The force correlation spectra for the narrow and wide wavepackets in the two energy regimes corresponding to oscillations in the classical potential as shown in Fig. 6. The spectra for the wide wavepacket are shifted for clarity.

correlation spectra at 13.67 and 0.67 eV, respectively. This is the case for both narrow as well as wide initial wavepackets. The 0.67 eV peak lies well within the wavepacket flux spectrum seen in Ref. 104, which depicts the collective motion of the electrons through the nanowire, whereas the 13.67 eV peak is close to the Fermi energy level of the Al electrode (11.6 eV).

C. Influence of external AC fields

In this subsection, we benchmark the MS-AIWD formalism, including coupled electron-nuclear dynamics in the presence of an external field. We benchmarked the MS-AIWD formalism by applying an oscillating electric field along internuclear axis of the Al_{54}C_7 nanowire with a frequency, $\omega = 0.22$ a.u. = 1.447 fs $^{-1}$, corresponding to the energy difference between the lowest two eigenstates of the electron-nuclear potential localized in the electrode region and a phase of $\phi = 3\pi/2$ so that the electric field starts from zero. The HOMO–LUMO gap in the $\text{Al}_{27} - \text{C}_7 - \text{Al}_{27}$ wire calculated at the B3LYP/6-31++G(D,P) level of theory is 0.0089 hartrees, while that of the $\text{Al}_6 - \text{C}_7 - \text{Al}_6$ molecule is 0.013 hartrees. In addition, the Fermi energy level of the Al electrode is 11.6 eV or 0.426 hartrees. We benchmark our approach by applying various electric fields and defining strong fields as those with energy greater than the Fermi energy of the electrode and weak fields as those with energy less than the HOMO–LUMO gap for the molecule. In Table III, we list the various electric field strengths and the corresponding intensities that are used for the following benchmarks.

In Fig. 8, we plot the average momenta for the narrow and wide wavepackets as a function of applied electric field, while in Fig. 9, we plot the average wavepacket density in the momentum representation. At low fields (below 0.01 a.u.), the average momentum is roughly constant. [Note that the grid

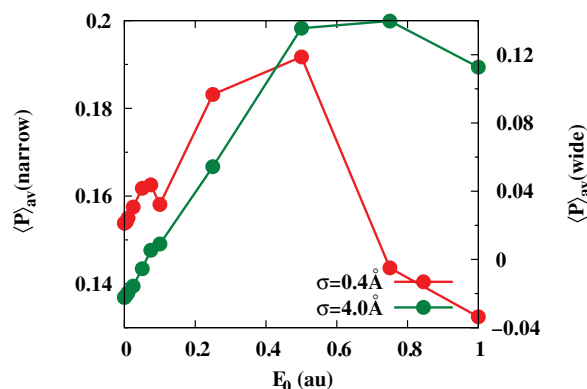


FIG. 8. Comparison of the time average of the expectation values of the wavepacket momentum, $\langle P \rangle_{av} = 1/T \int_0^T dt \langle \chi(t) | \hat{p} | \chi(t) \rangle$, as a function of applied electric field strength. The momenta are in atomic units, with the left axis describing the narrow wavepacket and the right axis describing the wide wavepacket.

spacing in the momentum representation is 0.02 a.u. which introduces a numerical uncertainty of a similar order.] This is also reflected in the behavior of the wavepacket density in the momentum representation. [See bottom three panels of Fig. 9 as well as Figs. 10(a), 10(b), 10(e), and 10(f).] Furthermore, as is to be expected, Figs. 10(a), 10(b), 10(e), and 10(f) are quite similar to the corresponding field-free results in Fig. 4. That is, in the low-field regime, the system behaves quite similar to field-free limit. This aspect is also reflected in the behavior of the transmission probability (that is the probability density in stage III) as a function of electric field strength as shown in Fig. 11. This implies that the electric field has very little effect on electron transport, which should be the case since the field is too weak to bring about electronic transitions and hence a difference in the electron transport mechanism.

For intermediate electric field strength, Fig. 8 indicates that the average momentum increases almost linearly (i.e., Ohmic behavior) with increasing field strength. This is true for both narrow as well as wide wavepackets. This aspect is consistent with Fig. 9, which indicates a corresponding increase in the amplitude of the wavepacket density in the positive momentum region. However, for stronger field strengths, the average momentum (Fig. 8) does not increase monotonically, but instead first plateaus out at $E_0 = 0.5$ a.u. or around the Fermi energy level of the electrode. Further increase in field strength leads to a reduction in average momentum. This is due to the relative decrease in the amplitude of average density for the momentum eigenvalues above 0.5 a.u., as seen in the top panels in Fig. 9. [This is similar to the field-free case shown in Fig. 5.] Furthermore, a sample of this

TABLE III. Electric ac field parameters used to benchmark MS-AIWD.

	Weak field				Intermediate field				Strong field		
E_0^a	0.001	0.005	0.01	0.025	0.05	0.075	0.1	0.25	0.5	0.75	1.0
$E_0/10^{10}$ ^b	0.051	0.257	0.514	1.286	2.571	3.857	5.142	12.855	25.711	38.567	51.422
$I = \frac{\epsilon_0 c E_0^2}{2} / 10^{16}$ ^c	0.035	0.877	3.509	21.934	87.736	197.41	350.94	2193.403	8773.61	19740.63	35094.45

^aUnits: atomic units.

^bUnits: V m $^{-1}$.

^cUnits: W m $^{-2}$.

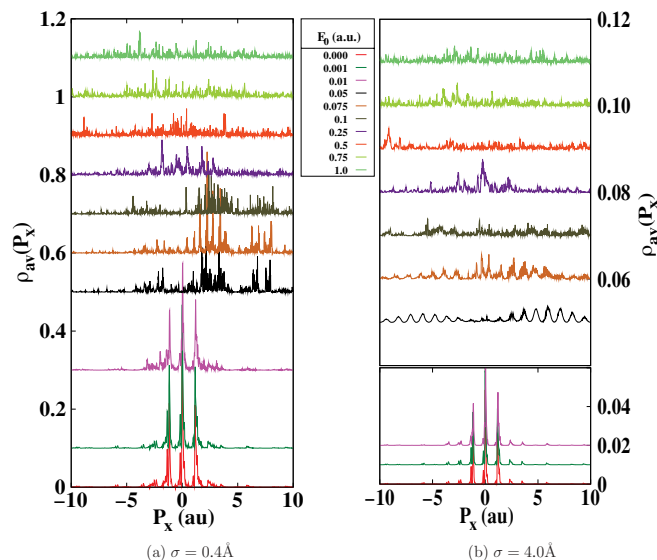


FIG. 9. Plot of the average wavepacket density in the momentum representation for (a) narrow wavepacket with $\sigma = 0.4 \text{ \AA}$ and (b) wide wavepacket with $\sigma = 4.0 \text{ \AA}$.

dissipative process is provided in Figs. 10(c), 10(d), and 10(g), and 10(h). In terms of the transmission probability, this is depicted by a steady shift in the peak around 1 fs toward smaller time-scales. This implies that the electron wavepacket is entering the stage III region or the acceptor side at earlier times.

A possible reason for this reduction in average momentum with field strength, for the stronger fields, can be understood as follows. As the electric field strength approaches the Fermi energy of the electrode, the wavepacket is completely delocalized over the entire momentum space, as seen in Fig. 9. This leads to roughly equal contributions from negative and positive momentum eigenstates and subsequently leads to a reduction in average momentum. For the transmission prob-

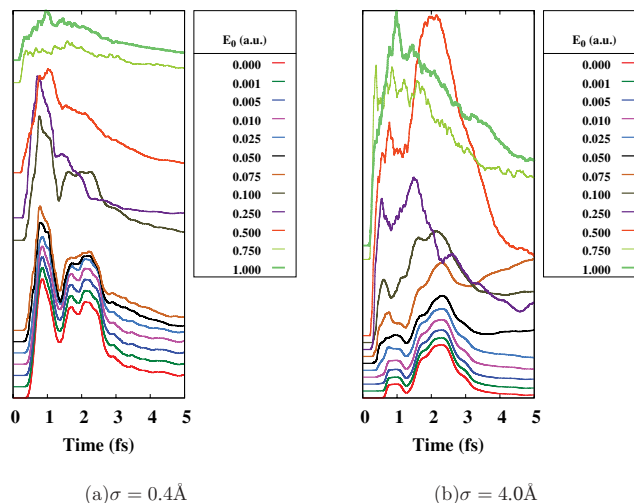


FIG. 11. Evolution of the transmission probability for the calculations outlined in Fig. 8.

ability, this is reflected by a broad spread for both the narrow and wide wavepackets, as seen in Fig. 11. It is interesting that such a complex behavior of electron transport can be obtained from the simple model for electron transport in open system dealt with here.

VII. CONCLUSION

In this paper we have generalized our recently developed multistage *ab initio* wavepacket dynamics¹⁰⁴ formalism to include coupled electron-nuclear dynamics and interaction with electromagnetic fields for electronically open systems. The MS-AIWD method entails the partitioning of a full donor-bridge-acceptor open system using judiciously placed offsetting absorbing and emitting potentials. Partitioning into multiple “stages,” based on the positions of the absorbing and emitting potentials allows accurate and efficient calculations

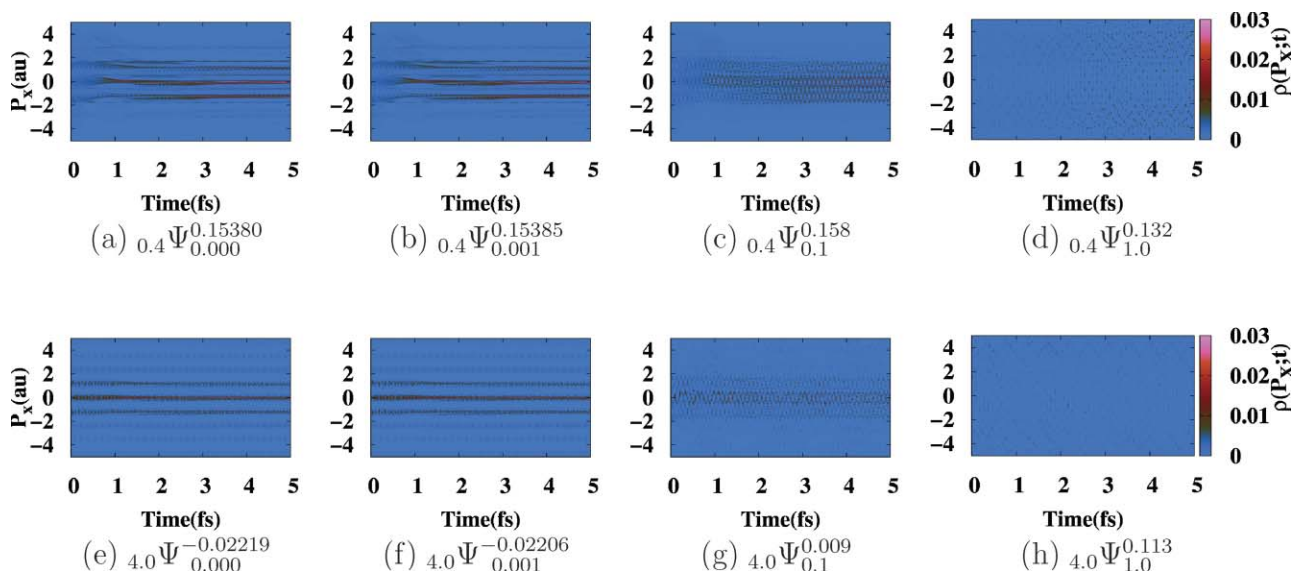


FIG. 10. Contour wavepacket density maps as in Fig. 4. The subfigure indices now include the electric field amplitude (in a.u.) as the right subscript. Strong electric fields result in a delocalized wavepacket, while weaker fields produce a wavepacket whose distribution remains unperturbed with respect to those in Fig. 4.

for semi-infinite systems by analyzing individual regions while preserving the coupling between the multiple spatial domains. In Ref. 104, we benchmarked the formalism using wavepackets with various widths and initial momenta. We showed that we could correctly reproduce the dynamics of the full system in the absence of partitioning.

Here, we first analyze the wavepacket in the momentum representation to provide further insight into the dynamics. Specifically, it is found that the uncertainty of the wavepacket in the momentum representation has a significant role in determining whether the dependence of average wavepacket momentum (that is parameters related to current flow) on the initial momentum (that is parameters related to bias) is monotonic or not. Upon further extending the MS-AIWD formalism to include coupled electron-nuclear dynamics and external fields, we find that this dependence persists. Based on our analysis we are able to categorize the behavior in the presence of weak, intermediate, and strong fields differently.

ACKNOWLEDGMENTS

This research is supported by the National Science Foundation grant NSF CHE-0750326 (S.S.I.). A.B.P. acknowledges Dr. Alexander Prociuk and Dr. Xiaohu Li for fruitful discussions and University Information Technology Services at Indiana University for supercomputing resources.

APPENDIX: EFFICIENT IMPLEMENTATIONS FOR DAF QUANTUM PROPAGATION

We have implemented a scheme which takes advantage of the attractive numerical properties of the banded Toeplitz matrix and greatly reduces the computational expense in the quantum propagation. Since the DAF propagator in Eq. (42) only depends on $(R_{QM}^i - R_{QM}^j)/\Delta x$, there exists a finite spatial width to the DAF propagator. If this width is denoted to include W grid points, then it is only necessary to store W elements of the DAF matrix, in each dimension, to ob-

tain the result of a propagation. This reduces the computational storage expense to be independent of N , where N is the number of grid points used in the discretization scheme. Second, instead of carrying out $\mathcal{O}(N^2)$ operations for computing Eq. (42) through matrix multiplication operations or $\mathcal{O}(N \log N)$ operations when implemented using Fourier transforms, we developed an algorithm which scales as $\mathcal{O}(N)$. We carry out a series of scalar-vector operations with the total number of operations in our scheme given by

$$N + \sum_{i=1}^{W-1} 2(N-i) = N(2W-1) - W(W-1) \approx \mathcal{O}(N), \quad (\text{A1})$$

where as noted earlier, W , the width of the propagator in the coordinate representation, is the maximum value of $(R_{QM}^i - R_{QM}^j)/\Delta x$ in Eq. (42) such that all values of the free-propagator are less than a numerical threshold for $(R_{QM}^i - R_{QM}^j)/\Delta x > W$. Since W does not depend on N [W in fact depends on M_{DAF} and $\sigma'(0)$, that is the required accuracy of propagation], this scaling goes as $\mathcal{O}(N)$ for large grids compared with $\mathcal{O}(N^2)$ for the matrix product implementation or $\mathcal{O}(N \log N)$ for implementation that makes use of Fourier transforms to solve Eq. (41).

The computational scaling discussed above does not include the effort involved in pre-computing the DAF elements. The required W elements of the DAF-propagator are computed once and stored, to be reused at every time step. The total cost involved in this operation is $W * M_{DAF}$, independent of problem size, N , and completely determined by the desired accuracy determined by choice of M_{DAF} and $\sigma'(0)$.

The reduction in computational cost discussed above is facilitated by converting Eq. (42) into a sequence of level-2 BLAS, vector operations,¹⁹⁶ where the full wavepacket, $\Psi(R_{QM}^i; t + \Delta t)$ is written in vector form as

$$\Psi_{t+\Delta t} = \Psi_{t+\Delta t} + \tilde{K}_{\sigma'(0), M_{DAF}}(R_{QM}^i - R_{QM}^j; \Delta t) \Psi_t. \quad (\text{A2})$$

This essentially constitutes a sequence of W , “aX+Y” operations, where “a” is a number and “X” and “Y” are vectors. Thus there are only $\mathcal{O}(W)$ such operations, each of which scale linearly in $\mathcal{O}(N)$, the overall scaling reduces to that in Eq. (A1). We utilize standard LAPACK and BLAS routines to carry out numerical implementation. Hence, the algorithm depicted by Eq. (A2) is represented as ZAXPY, the routine in level-2 BLAS used to carry out this operation, in Fig. 12. In Fig. 12, we provide a comparison of computational expense between the two propagation schemes: that is, the direct, $\mathcal{O}(N^2)$, implementation of Eq. (42) and that given by Eq. (A2). Clearly, the new algorithm is superior by several orders of magnitude. [The implementation here is also amicable to utilization of parallel BLAS libraries since both the $\mathcal{O}(W)$ and $\mathcal{O}(N)$ portions of the above algorithm are essentially decoupled. These aspects have not been included in the current implementation.]

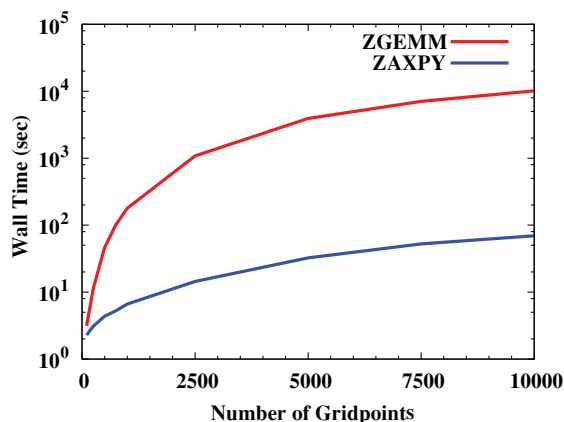


FIG. 12. Comparison of performance for the direct $\mathcal{O}(N^2)$ implementation of Eq. (42) (labeled “ZGEMM based algorithm”) with that given in Eqs. (A1) and (A2) (labeled “ZAXPY based algorithm”) for a 10 ps MS-AIWD dynamics trajectory. Clearly the scheme given by Eqs. (A1) and (A2) provides about 2 orders of magnitude improvement in computational expense for $N > 1000$, which represents the order of the problem treated in this paper.

¹H. B. Gray and J. R. Winkler, *Annu. Rev. Biochem.* **65**, 537 (1996).

²Y. Xiao, F. Patolsky, E. Katz, J. F. Hainfeld, and I. Willner, *Science* **299**, 1877 (2003).

³M. R. Wasielewski, *Chem. Rev.* **92**, 435 (1992).

- ⁴D. Gust, T. A. Moore, and A. L. Moore, *Acc. Chem. Res.* **34**, 40 (2001).
- ⁵H. Imahori, Y. Mori, and Y. Matano, *J. Photochem. Photobiol. C* **4**, 51 (2003).
- ⁶Y. Shirota, *J. Mater. Chem.* **10**, 1 (2000).
- ⁷P. Bonhote, A.-P. Dias, N. Papageorgiou, K. Kalyanasundaram, and M. Gratzel, *Inorg. Chem.* **35**, 1168 (1996).
- ⁸L. Schmidt-Mende, A. Fechtenkötter, K. Mullen, E. Moons, R. H. Friend, and J. D. Mackenzie, *Science* **293**, 1119 (2001).
- ⁹B. Thompson and J. fr chet, *Angew. Chem., Int. Ed.* **47**, 58 (2008).
- ¹⁰A. J. Nozik, *Physica E-Low-Dimensional Systems & Nanostructures* **14**(1–2), 115–120 (2002).
- ¹¹B. Tian, X. Zheng, T. J. Kempa, Y. Fang, N. Yu, G. Yu, J. Huang, and C. M. Lieber, *Nature (London)* **449**, 885 (2007).
- ¹²J. L. Segura, N. Martin, and D. M. Guldi, *Chem. Soc. Rev.* **34**, 31 (2005).
- ¹³J. Nelson, *Curr. Opin. Solid State Mater. Sci.* **6**, 87 (2002).
- ¹⁴N. Robertson, *Angew. Chem., Int. Ed.* **45**, 2338 (2006).
- ¹⁵J. Bisquert, D. Cahen, G. Hodes, S. R hle, and A. Zaban, *J. Phys. Chem. B* **108**, 8106 (2004).
- ¹⁶A. Goetzberger, C. Hebling, and H.-W. Schock, *Mater. Sci. Eng. R.* **40**, 1 (2003).
- ¹⁷D. M. Adams, L. Brus, C. E. D. Chidsey, S. Creager, C. Creutz, C. R. Kagan, P. V. Kamat, M. Lieberman, S. Lindsay, R. A. Marcus, R. Metzger, M. E. Michel-Beyerle, J. R. Miller, M. D. Newton, D. R. Rolison, O. Sankey, K. S. Schanze, J. Yardley, and X. Zhu, *J. Phys. Chem. B* **107**, 6668 (2003).
- ¹⁸N. Tessler, V. Medvedev, M. Kazes, S. Kan, and U. Banin, *Science* **295**, 1506 (2002).
- ¹⁹E. Baranoff, J.-P. Collin, L. Flamigni, and J.-P. Sauvage, *Chem. Soc. Rev.* **33**, 147 (2004).
- ²⁰T. Konishi, A. Ikeda, and S. Shinkai, *Tetrahedron* **61**, 4881 (2005).
- ²¹N. S. Lewis and D. G. Nocera, *Proc. Natl. Acad. Sci. U.S.A.* **103**, 15729 (2006).
- ²²S. Fukuzumi, *Bull. Chem. Soc. Jpn.* **79**, 177 (2006).
- ²³J. Jortner, M. Bixon, T. Langenbacher, and M. E. Michel-Beyerle, *Proc. Natl. Acad. Sci. U.S.A.* **95**, 12759 (1998).
- ²⁴S. O. Kelley and J. K. Barton, *Science* **283**, 375 (1999).
- ²⁵H.-W. Fink and C. Schonberger, *Nature (London)* **398**, 407 (1999).
- ²⁶M. Ratner, *Nature (London)* **397**, 480 (1999).
- ²⁷P. Tran, B. Alavi, and G. Gruner, *Phys. Rev. Lett.* **85**, 1564 (2000).
- ²⁸A. Y. Kasumov, M. Kociak, S. Gueron, B. Reulet, V. T. Volkov, D. V. Klinov, and H. Bouchiat, *Science* **291**, 280 (2001).
- ²⁹J. Jortner, M. Bixon, A. A. Voityuk, and N. Rosch, *J. Phys. Chem. A* **106**, 7599 (2002).
- ³⁰D.-F. Feng and L. Kevan, *Chem. Rev.* **80**, 1 (1980).
- ³¹M. Sprik, R. W. Impey, and M. L. Klein, *J. Chem. Phys.* **83**, 5802 (1985).
- ³²R. N. Barnett, U. Landman, and A. Nitzan, *J. Chem. Phys.* **89**, 2242 (1988).
- ³³A. Wallqvist, G. Martyna, and B. J. Berne, *J. Phys. Chem.* **92**, 1721 (1988).
- ³⁴F. H. Long, H. Lu, and K. B. Eisenthal, *Phys. Rev. Lett.* **64**, 1469 (1990).
- ³⁵H. Abramczyk and J. Kroh, *J. Phys. Chem.* **95**, 5749 (1991).
- ³⁶P. Ayotte and M. A. Johnson, *J. Chem. Phys.* **106**, 811 (1997).
- ³⁷L. Turi, A. Mosyak, and P. J. Rossky, *J. Chem. Phys.* **107**, 1970 (1997).
- ³⁸N. I. Hammer, J.-W. Shin, J. M. Headrick, E. G. Diken, J. R. Roscioli, G. H. Weddle, and M. A. Johnson, *Science* **306**, 675 (2004).
- ³⁹J. R. R. Verlet, A. E. Bragg, A. Kammrath, O. Cheshnovsky, and D. M. Neumark, *Science* **307**, 93 (2005).
- ⁴⁰J. M. Herbert and M. Head-Gordon, *Proc. Natl. Acad. Sci. U.S.A.* **103**, 14282 (2006).
- ⁴¹K. R. Asmis, G. Santambrogio, J. Zhou, E. Garand, J. Headrick, D. Goebbert, M. A. Johnson, and D. M. Neumark, *J. Chem. Phys.* **126**, 191105 (2007).
- ⁴²A. Nitzan and M. A. Ratner, *Science* **300**, 1384 (2003).
- ⁴³A. Troisi and M. A. Ratner, *Small* **2**, 172 (2006).
- ⁴⁴D. James and J. Tour, *Chem. Mater.* **16**, 4423 (2004).
- ⁴⁵R. McCreery, *Chem. Mater.* **16**, 4477 (2004).
- ⁴⁶J. R. Heath and M. A. Ratner, *Phys. Today* **56**(5), 43 (2003).
- ⁴⁷M. A. Reed, *Nature Mater.* **3**, 286 (2004).
- ⁴⁸C. Joachim and M. A. Ratner, *Proc. Natl. Acad. Sci. U.S.A.* **102**, 8801 (2005).
- ⁴⁹J. R. Reimers, A. Bilic, Z. L. Cai, M. Dahlbom, N. A. Lambropoulos, G. C. Solomon, M. J. Crossley, and N. S. Hush, *Aust. J. Chem.* **57**, 1133 (2004).
- ⁵⁰N. A. Melosh, A. Boukai, F. Diana, B. Gerardot, A. Badolato, P. M. Petroff, and J. R. Heath, *Science* **300**, 112 (2003).
- ⁵¹R. A. Beckman, E. Johnston-Halperin, N. A. Melosh, Y. Luo, J. E. Green, and J. R. Heath, *J. Appl. Phys.* **96**, 5921 (2004).
- ⁵²E. W. Wong, C. P. Collier, M. Behloradsky, F. M. Raymo, J. F. Stoddart, and J. Heath, *J. Am. Chem. Soc.* **122**, 5831 (2000).
- ⁵³J. Tour, *Acc. Chem. Res.* **33**, 791 (2000).
- ⁵⁴J. Lindsey, *New J. Chem.* **15**, 153–180 (1991).
- ⁵⁵J. R. Bolton, Jr., *Sol. Energy* **57**, 37 (1996).
- ⁵⁶J. R. Bolton, Jr., and D. Hall, *Ann. Rev. Energy* **4**, 353 (1979).
- ⁵⁷J. Hurley and G. Tollin, *Sol. Energy* **28**, 187 (1982).
- ⁵⁸S. Kobayashi, T. Nishikawa, T. Takenobu, S. Mori, T. Shimoda, T. Mitani, H. Shimotani, N. Yoshimoto, S. Ogawa, and Y. Iwasa, *Nature Mater.* **3**, 317 (2004).
- ⁵⁹S. T. Bromley, M. Mas-Torrent, P. Hadley, and C. Rovira, *J. Am. Chem. Soc.* **126**, 6544 (2004).
- ⁶⁰R. G. Endres, D. L. Cox, and R. R. P. Singh, *Rev. Mod. Phys.* **76**, 195 (2004).
- ⁶¹S. F. Nelson, Y.-Y. Lin, D. J. Gundlach, and T. N. Jackson, *Appl. Phys. Lett.* **72**, 1854 (1998).
- ⁶²E. A. Weiss, M. J. Ahrens, L. E. Sinks, A. V. Gusev, M. A. Ratner, and M. R. Wasielewski, *J. Am. Chem. Soc.* **126**, 5577 (2004).
- ⁶³M. Soljai and J. D. Joannopoulos, *Nature Mater.* **3**, 211 (2004).
- ⁶⁴M. Heilemann, P. Tinnefeld, G. S. Mozeiro, M. G. Parajo, N. F. V. Hulst, and M. Sauer, *J. Am. Chem. Soc.* **126**, 6514 (2004).
- ⁶⁵Z. H. Donhauser, B. A. Mantooh, K. F. Kelly, L. A. B. J. D. Monnell, J. J. Stapleton, D. W. Price, A. M. Rawlett, D. L. Allara, J. M. Tour, and P. S. Weiss, *Science* **292**, 2303 (2001).
- ⁶⁶L. A. Bumm, J. J. Arnold, M. T. Cygan, T. D. Dunbar, T. P. Burgin, L. Jones, II., D. L. Allara, J. M. Tour, and P. S. Weiss, *Science* **271**, 1705 (1996).
- ⁶⁷A. H. Flood, R. J. A. Ramirez, W. Q. Deng, R. P. Muller, W. A. Goddard, and J. F. Stoddart, *Aust. J. Chem.* **57**, 301 (2004).
- ⁶⁸C. Zhou, M. Deshpande, M. Reed, L. Jones, and J. Tour, *Appl. Phys. Lett.* **71**, 611 (1997).
- ⁶⁹T. Lee, W. Wang, and M. Reed, *Jpn. J. Appl. Phys., Part 1* **44**, 523 (2005).
- ⁷⁰M. L. Chabinyc, X. X. Chen, R. E. Holmlin, H. Jacobs, H. Skulason, C. D. Frisbie, V. Mujica, M. A. Ratner, M. A. Rampi, and G. M. Whitesides, *J. Am. Chem. Soc.* **124**, 11730 (2002).
- ⁷¹J. Chen, M. Reed, A. Rawlett, and J. Tour, *Science* **286**, 1550 (1999).
- ⁷²Y. H. Kim, S. S. Jang, and W. A. Goddard, *J. Chem. Phys.* **122**, 244703 (2005).
- ⁷³S. Tans, A. R. M. Verschueren, and C. Dekker, *Nature (London)* **393**, 49 (1998).
- ⁷⁴A. Y. Kasumov, R. Deblock, M. Kociak, B. Reulet, H. Bouchiat, I. I. Khodos, Y. B. Gorbatov, V. T. Volkov, C. Journet, and M. Burghard, *Science* **284**, 1508 (1999).
- ⁷⁵Z. K. Tang, L. Y. Zhang, N. Wang, X. X. Zhang, G. H. Wen, G. D. Li, J. N. Wang, C. T. Chan, and P. Sheng, *Science* **292**, 2462 (2001).
- ⁷⁶J. P. Hill, W. S. Jin, A. Kosaka, T. Fukushima, H. Ichihara, T. Shimomura, K. Ito, T. Hashizume, N. Ishii, and T. Aida, *Science* **304**, 1481 (2004).
- ⁷⁷A. Nitzan, *Annu. Rev. Phys. Chem.* **52**, 681 (2001).
- ⁷⁸S. Datta, *Quantum Transport Atom to Transistor* (Cambridge University Press, Cambridge, 2005).
- ⁷⁹L. V. Keldysh, *Sov. Phys. JETP-USSR* **20**(4), 1018 (1965).
- ⁸⁰L. P. Kadanoff and G. Baym, *Quantum Statistical Mechanics. Green's Function Methods in Equilibrium Problems* (Benjamin, New York, 1962).
- ⁸¹V. Mujica, M. Ratner, and O. Goswami, *Int. J. Quantum Chem.* **90**, 14 (2002).
- ⁸²P. Daml , A. W. Ghosh, and S. Datta, *Chem. Phys.* **281**, 171 (2002).
- ⁸³Y. Q. Xue, S. Datta, and M. A. Ratner, *Chem. Phys.* **281**, 151 (2002).
- ⁸⁴V. Mujica, M. Kemp, and M. A. Ratner, *J. Chem. Phys.* **101**, 6849 (1994).
- ⁸⁵V. Mujica, M. Kemp, and M. A. Ratner, *J. Chem. Phys.* **101**, 6856 (1994).
- ⁸⁶S. Alavi, B. Larade, J. Taylor, H. Guo, and T. Seideman, *Chem. Phys.* **281**, 293 (2002).
- ⁸⁷T. Seideman and H. Guo, *Theor. Comput. Chem.* **2**, 439 (2003).
- ⁸⁸N. Sergueev, D. Roubtsov, and H. Guo, *Phys. Rev. Lett.* **95** (2005).
- ⁸⁹S. Ke, H. Baranger, and W. Yang, *J. Chem. Phys.* **123**, 114701 (2005).
- ⁹⁰A. P. Horsfield, D. R. Bowler, and A. J. Fisher, *J. Phys.: Condens. Matter* **16**, L65 (2004).
- ⁹¹M. Brandbyge, T. J. Schio, R. M. R. So, P. Stoltze, K. W. Jacobsen, R. J. K. No, L. Olesen, E. Laegsgaard, I. Stensgaard, and F. Besenbacher, *Phys. Rev. B* **52**, 8499 (1995).

- ⁹²D. R. Bowler, A. P. Horsfield, C. G. Sánchez, and T. N. Todorov, *J. Phys.: Condens. Matter* **17**, 3985 (2005).
- ⁹³Y. Dahnovsky, V. G. Zakrzewski, A. Kletsov, and J. V. Ortiz, *J. Chem. Phys.* **123**, 184711 (2005).
- ⁹⁴Y. Dahnovsky and J. V. Ortiz, *J. Chem. Phys.* **124**, 144114 (2006).
- ⁹⁵C. Verdozzi, G. Stefanucci, and C. Almbladh, *Phys. Rev. Lett.* **97**, 046603 (2006).
- ⁹⁶C.-L. Cheng, J. S. Evans, and T. V. Voorhis, *Phys. Rev. B* **74**, 155112 (2006).
- ⁹⁷M. Koentopp, K. Burke, and F. Evers, *Phys. Rev. B* **73**, 121403 (2006).
- ⁹⁸E. J. Mcenery, D. R. Bowler, D. Dundas, A. P. Horsfield, C. G. Sánchez, and T. N. Todorov, *J. Phys.: Condens. Matter* **19**, 196201 (2007).
- ⁹⁹A. Prociuk and B. D. Dunietz, *Phys. Rev. B* **78**, 165112 (2008).
- ¹⁰⁰S. Kurth, G. Stefanucci, C.-O. Almbladh, A. Rubio, and E. K. U. Gross, *Phys. Rev. B* **72**, 035308 (2005).
- ¹⁰¹J. Jiang, M. Kula, and Y. Luo, *J. Chem. Phys.* **124**, 034708 (2006).
- ¹⁰²K. Burke, R. Car, and R. Gebauer, *Phys. Rev. Lett.* **94**, 146803 (2005).
- ¹⁰³J. Yuen-Zhou, D. G. Tempel, C. A. Rodríguez-Rosario, and A. Aspuru-Guzik, *Phys. Rev. Lett.* **104**, 043001 (2010).
- ¹⁰⁴A. Pacheco and S. S. Iyengar, *J. Chem. Phys.* **133**, 044105 (2010).
- ¹⁰⁵T. Peng and J. Z. H. Zhang, *J. Chem. Phys.* **105**, 6072 (1996).
- ¹⁰⁶D. J. Kouri, D. K. Hoffman, T. Peng, and J. H. Z. Zhang, *Chem. Phys. Lett.* **262**, 519 (1996).
- ¹⁰⁷W. Zhu, T. Peng, and J. Z. H. Zhang, *J. Chem. Phys.* **106**, 1742 (1997).
- ¹⁰⁸S. C. Althorpe, D. J. Kouri, and D. K. Hoffman, *J. Chem. Phys.* **107**, 7816 (1997).
- ¹⁰⁹Y. C. Zhang, J. F. Zhang, H. Y. Zhang, Q. G. Zhang, and J. Z. H. Zhang, *J. Chem. Phys.* **115**, 8455 (2001).
- ¹¹⁰S. C. Althorpe, *J. Chem. Phys.* **114**, 1601 (2001).
- ¹¹¹S. C. Althorpe and D. C. Clary, *Annu. Rev. Phys. Chem.* **54**, 493 (2003).
- ¹¹²S. C. Althorpe, *Phys. Rev. A* **69**, 042702 (2004).
- ¹¹³Y. Zhang, T.-X. Xie, K.-L. Han, and J. Z. H. Zhang, *J. Chem. Phys.* **124**, 134301 (2006).
- ¹¹⁴M. T. Cvitas and S. C. Althorpe, *Phys. Scr.* **80** (2009).
- ¹¹⁵M. T. Cvitas and S. C. Althorpe, *J. Phys. Chem. A* **113**, 4557 (2009).
- ¹¹⁶Z. Sun, D. H. Zhang, and M. H. Alexander, *J. Chem. Phys.* **132**, 034308 (2010).
- ¹¹⁷R. C. Mowrey and D. J. Kouri, *J. Chem. Phys.* **84**, 6466 (1986).
- ¹¹⁸D. Neuhauser, M. Baer, R. S. Judson, and D. J. Kouri, *Comput. Phys. Commun.* **63**, 460 (1991).
- ¹¹⁹T. N. Todorov, J. Hoekstra, and A. P. Sutton, *Philos. Mag. B* **80**, 421 (2000).
- ¹²⁰M. D. Ventra, S. T. Pantelides, and N. D. Lang, *Phys. Rev. Lett.* **88**, 046801 (2002).
- ¹²¹F. Evers, F. Weigend, and M. Koentopp, *Phys. Rev. B* **69**, 235411 (2004).
- ¹²²A. P. Sutton and T. N. Todorov, *Mol. Phys.* **102**, 919 (2004).
- ¹²³W. H. Weinberg, *Annu. Rev. Phys. Chem.* **29**, 115 (1978).
- ¹²⁴S. K. Khanna and J. Lambe, *Science* **220**, 1345 (1983).
- ¹²⁵W. Wang, T. Lee, I. Kretzschmar, and M. Reed, *Nano Lett.* **4**, 643 (2004).
- ¹²⁶J. Kushmerick, J. Lazorcik, C. Patterson, R. Shashidhar, D. Seferos, and G. Bazan, *Nano Lett.* **4**, 639 (2004).
- ¹²⁷M. Galperin, M. A. Ratner, and A. Nitzan, *J. Chem. Phys.* **121**, 11965 (2005).
- ¹²⁸A. Goldberg and B. W. Shore, *J. Phys. B* **11**, 3339 (1978).
- ¹²⁹C. Leforestier and R. E. Wyatt, *J. Chem. Phys.* **78**, 2334 (1983).
- ¹³⁰R. Kosloff and D. Kosloff, *J. Comput. Phys.* **63**, 363 (1986).
- ¹³¹D. Neuhauser and M. Baer, *J. Chem. Phys.* **90**, 4351 (1989).
- ¹³²T. Seideman and W. H. Miller, *J. Chem. Phys.* **96**, 4412 (1992).
- ¹³³T. Seideman and W. H. Miller, *J. Chem. Phys.* **97**, 2499 (1992).
- ¹³⁴W. P. Reinhardt, *Annu. Rev. Phys. Chem.* **33**, 223 (1982).
- ¹³⁵N. Moiseyev, *J. Phys. B* **31**, 1431 (1998).
- ¹³⁶N. Moiseyev, *Phys. Rep.* **302**, 212 (1998).
- ¹³⁷R. Zavin, I. Vorobeichik, and N. Moiseyev, *Chem. Phys. Lett.* **288**, 413 (1998).
- ¹³⁸J. G. Muga, J. P. Palao, B. Navarro, and I. L. Egusquiza, *Phys. Rep.* **395**, 357 (2004).
- ¹³⁹A. Fleischer and N. Moiseyev, *Phys. Rev. A* **72**, 032103 (2005).
- ¹⁴⁰O. Shemer, D. Brisker, and N. Moiseyev, *Phys. Rev. A* **71**, 032716 (2005).
- ¹⁴¹Y. Sajeev, M. Sindelka, and N. Moiseyev, *Chem. Phys.* **329**, 307 (2006).
- ¹⁴²D. Macías, S. Brouard, and J. G. Muga, *Chem. Phys. Lett.* **228**, 672 (1994).
- ¹⁴³M. Child, *Mol. Phys.* **72**, 89 (1991).
- ¹⁴⁴U. V. Riss and H.-D. Meyer, *J. Chem. Phys.* **105**, 1409 (1996).
- ¹⁴⁵P. Pfeifer and R. D. Levine, *J. Chem. Phys.* **79**, 5512 (1983).
- ¹⁴⁶A. Vibok and G. G. Balint-Kurti, *J. Chem. Phys.* **96**, 7615 (1992).
- ¹⁴⁷J.-P. Berenger, *J. Comput. Phys.* **114**, 185 (1994).
- ¹⁴⁸B. Alpert, L. Greengard, and T. Hagstrom, *J. Comput. Phys.* **180**, 270 (2002).
- ¹⁴⁹J. Perie and G. Jolicard, *J. Phys. B* **26**, 4491 (1993).
- ¹⁵⁰U. V. Riss and H.-D. Meyer, *J. Phys. B* **26**, 4503 (1993).
- ¹⁵¹A. Vibok and G. G. Balint-Kurti, *J. Phys. Chem.* **96**, 8712 (1992).
- ¹⁵²B. Engquist and A. Majda, *Math. Comput.* **31**, 629 (1977).
- ¹⁵³A. M. Ermolaev, I. V. Puzynin, A. V. Selin, and S. I. Vinitzky, *Phys. Rev. A* **60**, 4831 (1999).
- ¹⁵⁴S. K. Maiti, *Phys. Lett. A* **362**, 225 (2007).
- ¹⁵⁵F. Evers and A. Arnold, "Molecular conductance from *ab initio* calculations: Self energies and absorbing boundary conditions," in CFN Lectures on Functional Nanostructures, Lecture Notes in Physics Vol. II (Springer, New York, 2010), condensed matter archive: <http://arxiv.org/abs/cond-mat/0611401v1>.
- ¹⁵⁶T. M. Henderson, G. Fagas, E. Hyde, and J. C. Greer, *J. Chem. Phys.* **125**, 244104 (2006).
- ¹⁵⁷F. Goyer, M. Ernzerhof, and M. Zhuang, *J. Chem. Phys.* **126**, 144104 (2007).
- ¹⁵⁸R. M. Dreizler and E. K. U. Gross, *Density Functional Theory: An Approach to the Quantum Many Body Problem* (Springer-Verlag, Berlin, 1990).
- ¹⁵⁹A.-P. Jauho, N. S. Wingreen, and Y. Meir, *Phys. Rev. B* **50**, 5528 (1994).
- ¹⁶⁰F. Maseras and K. Morokuma, *J. Comput. Chem.* **16**, 1170 (1995).
- ¹⁶¹S. Humbel, S. Sieber, and K. Morokuma, *J. Chem. Phys.* **105**, 1959 (1996).
- ¹⁶²M. Svensson, S. Humbel, R. D. J. Froese, T. Matsubara, S. Sieber, and K. Morokuma, *J. Phys. Chem.* **100**, 19357 (1996).
- ¹⁶³M. Svensson, S. Humbel, and K. Morokuma, *J. Chem. Phys.* **105**, 3654 (1996).
- ¹⁶⁴T. A. Wesolowski and A. Warshel, *J. Phys. Chem.* **97**, 8050 (1993).
- ¹⁶⁵P. N. Day, J. H. Jensen, M. S. Gordon, S. P. Webb, W. J. Stevens, M. Krauss, D. Garmer, H. Basch, and D. Cohen, *J. Chem. Phys.* **105**, 1968 (1996).
- ¹⁶⁶N. Govind, Y. A. Wang, A. J. R. da Silva, and E. A. Carter, *Chem. Phys. Lett.* **295**, 129 (1998).
- ¹⁶⁷H. P. Hratchian, P. V. Parandekar, K. Raghavachari, M. J. Frisch, and T. Vreven, *J. Chem. Phys.* **128**, 034107 (2008).
- ¹⁶⁸C. Kittel, *Introduction To Solid State Physics* (Wiley, New York, 1996).
- ¹⁶⁹J. Chen, W. Wang, M. A. Reed, A. M. Rawlett, D. W. Price, and J. M. Tour, *Appl. Phys. Lett.* **21**, 1224 (2000).
- ¹⁷⁰A. D. McLachlan, *Mol. Phys.* **8**, 39 (1964).
- ¹⁷¹K. C. Kulander, K. R. S. Devi, and S. E. Koonin, *Phys. Rev. A* **25**, 2968 (1982).
- ¹⁷²D. A. Micha, *J. Chem. Phys.* **78**, 7138 (1983).
- ¹⁷³Z. Kirson, R. B. Gerber, A. Nitzan, and M. A. Ratner, *Surf. Sci.* **137**, 527 (1984).
- ¹⁷⁴S.-I. Sawada, A. Nitzan, and H. Metiu, *Phys. Rev. B* **32**, 851 (1985).
- ¹⁷⁵K. C. Kulander, *Phys. Rev. A* **36**, 2726 (1987).
- ¹⁷⁶M. J. Field, *J. Chem. Phys.* **96**, 4583 (1992).
- ¹⁷⁷P. V. Parandekar and J. C. Tully, *J. Chem. Phys.* **122**, 094102 (2005).
- ¹⁷⁸X. Li, J. C. Tully, H. B. Schlegel, and M. J. Frisch, *J. Chem. Phys.* **123**, 084106 (2005).
- ¹⁷⁹C. M. Isborn, X. Li, and J. C. Tully, *J. Chem. Phys.* **126**, 134307 (2007).
- ¹⁸⁰W. C. Swope, H. C. Andersen, P. H. Berens, and K. R. Wilson, *J. Chem. Phys.* **76**, 637 (1982).
- ¹⁸¹A. K. Mazur, *J. Comput. Phys.* **136**, 354 (1997).
- ¹⁸²J. D. Jackson, *Classical Electrodynamics*, 3rd. ed. (Wiley, New York, 1999).
- ¹⁸³C. Cohen-Tannoudji, B. Diu, and F. Loloë, *Quantum Mechanics* (Wiley, New York, 1977), Vol. 2.
- ¹⁸⁴S. S. Iyengar and J. Jakowski, *J. Chem. Phys.* **122**, 114105 (2005).
- ¹⁸⁵S. S. Iyengar, *Theor. Chem. Acc.* **116**, 326 (2006).
- ¹⁸⁶J. Jakowski, I. Sumner, and S. S. Iyengar, *J. Chem. Theory Comput.* **2**, 1203 (2006).
- ¹⁸⁷I. Sumner and S. S. Iyengar, *J. Phys. Chem. A* **111**, 10313 (2007).
- ¹⁸⁸X. Li and S. S. Iyengar, *J. Chem. Phys.* **132**, 184105 (2010).
- ¹⁸⁹Y. Huang, D. J. Kouri, M. Arnold, I. Thomas L. Marchioro, and D. K. Hoffman, *Comput. Phys. Commun.* **80**, 1 (1994).

- ¹⁹⁰Y. Huang, W. Zhu, D. Kouri, and D. K. Hoffman, *J. Phys. Chem.* **98**, 1868 (1994).
- ¹⁹¹G. W. Wei, S. C. Althorpe, D. J. Kouri, and D. K. Hoffman, *J. Chem. Phys.* **108**, 7065 (1998).
- ¹⁹²G. W. Wei, S. C. Althorpe, D. S. Zhang, D. J. Kouri, and D. K. Hoffman, *Phys. Rev. A* **57**, 3309 (1998).
- ¹⁹³D. K. Hoffman, N. Nayar, O. A. Sharafeddin, and D. J. Kouri, *J. Phys. Chem* **95**, 8299 (1991).
- ¹⁹⁴D. K. Hoffman, M. Arnold, and D. J. Kouri, *J. Phys. Chem.* **96**, 6539 (1992).
- ¹⁹⁵G. D. Mahan, *Many Particle Physics (Physics of Solids and Liquids)* (Plenum, New York, 2000).
- ¹⁹⁶E. Anderson, Z. Bai, C. Bischof, S. Blackford, J. Demmel, J. Dongarra, J. D. Croz, A. Greenbaum, S. Hammarling, A. McKenney, A. Sorenson, and D. Sorensen, *LAPACK Users' Guide*, 3rd. ed. (Society for Industrial and Applied Mathematics, Philadelphia, PA, 1999).